

Effect of Tb³⁺ ions on the ZnO nanoparticles synthesized by chemical bath deposition method

Lehlohonolo F. Koao^{1*}, Birhanu F. Dejene¹, Hendrik C. Swart², Setumo V. Motlounge³, Tshwafo E. Motaung⁴, Shanganyane P. Hlangothi⁵

¹Department of Physics, University of the Free State (Qwaqwa Campus), Private Bag X13, Phuthaditjhaba, 9866, South Africa

²Department of Physics, University of the Free State, P. O. Box 339, Bloemfontein, 9300, South Africa

³Department of Physics, Sefako Makgatho Health Science University, P. O. Box 94, Medunsa, 0204, South Africa

⁴Department of Chemistry, University of Zululand, Guldengracht st & East Arterial Road, Richards Bay, 3900, South Africa

⁵Department of Chemistry, Nelson Mandela Metropolitan University, P.O. Box 77000, Port Elizabeth 6031, South Africa

*Corresponding author. Tel: (+27) 587185300; E-mail: koaolf@qwa.ufs.ac.za; koao@webmail.co.za

Received: 31 August 2015, Revised: 16 February 2016 and Accepted: 05 May 2016

ABSTRACT

Tb³⁺ doped ZnO nanoparticles were synthesized using the chemical bath deposition (CBD) method at 80 °C. All the samples were annealed at 700 °C to remove the hydroxyl groups confirmed by the thermogravimetric analysis (TGA) and differential thermogravimetric analysis (DTGA). The thermal analysis, structure, morphology and optical properties were characterized. The TGA and DTGA showed that the final yield decreases with an increase in the amount of molar concentration of Tb³⁺ ions. The X-ray diffraction (XRD) spectra of the ZnO: Tb³⁺ nanoparticles correspond to the various planes of hexagonal ZnO phase for the lower and higher Tb concentration samples. The estimated average grain sizes calculated using the XRD spectra were found to be in the order of 44 ± 2 nm. The grain size was found to increase with an increase in the amount of Tb³⁺ ions. Scanning electron microscopy (SEM) micrographs showed nanoparticles are obtained for undoped ZnO and emergence of pyramids shape for higher molar concentration of Tb³⁺ ions. The reflectance spectra depict a red shift with an increase in Tb³⁺ molar concentration. Photoluminescence (PL) results showed that the luminescence intensity increased with an increase in the amount of Tb³⁺ ions. Copyright © 2016 VBRI Press.

Keywords: CBD; Tb³⁺- ZnO; pyramids; luminescence.

Introduction

Zinc oxide (ZnO) semiconductors gathered a lot of attention nowadays because they are considered to be excellent host materials. ZnO is one of the very important II-VI group semiconductors that have a wide and direct band gap of 3.37 eV at room temperature and it has a large exciton binding energy of 60 meV [1]. As a result of its excellent chemical and physical properties [2], ZnO has been widely used in low-voltage phosphor material [3]. Doping ZnO nanoparticles have become an important issue in ZnO-based nano-material research due to the fact that doping elements can efficiently adjust their electrical, optical and magnetic properties, and results into various applications of ZnO based nano materials [4]. Doping with rare earth ions (RE³⁺) influence the morphology, the particle size and the band structure of the nanocrystals [4-5]. It is still a challenge that how does the change in shape of morphology affect the luminescence band and intensity. Doping also play key roles in luminescence efficiency and the position of emission bands thus influencing their practical applications. The enhanced luminescence of RE³⁺ ions is achieved by the efficient energy transfer from semiconductor host to rare earth ions

[6]. Doping ZnO with RE is still remains a challenge to achieve high quality of crystalline particles with excellent physical and chemical properties of doped ZnO nanostructures [7-8]. Due to potential optoelectronic applications, nowadays RE³⁺ doped ZnO are an interesting field of study [7]. Many RE³⁺ ions such as Tb³⁺, Ce³⁺, Gd³⁺, Er³⁺, Eu³⁺, Nd³⁺ and Pr³⁺ were doped as absorption and emission centres in semiconductor hosts [7, 9-14]. Among the RE³⁺ ions, Tb³⁺ is the most popular efficient luminescent material [5]. Particularly, Tb³⁺ could be used as phosphorous for fluorescent lamps and emission agents, or sensitizing agents for plasma displays. Efficient blue-green emission with a wide spectral tunability has been a key interest in optoelectronics. Reisfeld *et al.* [15] reported the significant increase in the emission of Tb³⁺ and Eu³⁺ doped ZrO₂ in the presence of CdS nanocrystals. The obtained results confirmed that the energy from nonradiative combination can be transferred to the high-lying excited energy levels of the Tb³⁺ and Eu³⁺ ions. This is followed by a nonradiative decay from the excited levels to the long-lived ⁵D₀ level of Eu³⁺ or the ⁵D₄ level of Tb³⁺, which is expected to increase the population of the emitting levels but not their emission probability to the ground state,

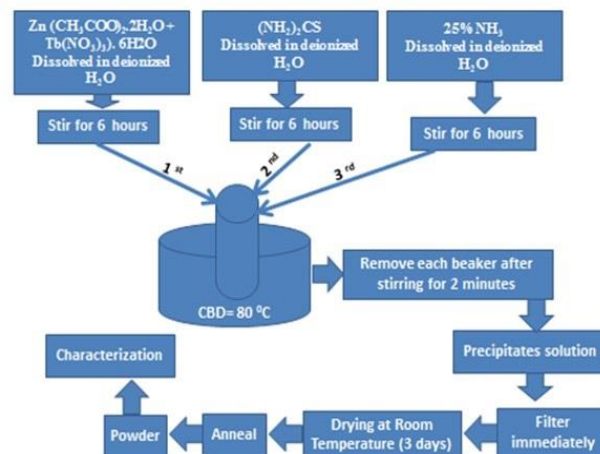
as confirmed by a similar decay time of Eu^{3+} ions, which was observed even after the addition of CdS nanocrystals. Kumar *et al.* [5] reported Tb-doped ZnO synthesized by combustion method. Photoluminescence studies showed the best luminescence intensity was for 5 mol % doped samples and further increasing the amount of dopant caused luminescence quenching. In this paper it was observed that the luminescence intensity increases with an increase in molar concentration of Tb^{3+} ions while the shape of morphology was changed from spherical nanoparticles to pyramids. In recent years, considerable efforts have been made to synthesize ZnO nanoparticles doped with Tb^{3+} by several methods such as solid state reaction [6], sol-gel [1], combustion [5], and electrodeposited method [16]. The chemical bath deposition (CBD) method is a simple, cheap and convenient process to prepare semiconducting materials. CBD is a low temperature technique which uses a solution (almost always aqueous) which produces a crystal size that is often very small and homogeneous. In this work, the Tb-doped ZnO nanoparticles were prepared by low temperature CBD method. Currently, the production of high-quality phosphors for white-light-emitting applications is a hot topic in the phosphor material synthesis research around the world due to the important goals such as; for the light-emitting diodes (LEDs) in the market and possible applications in households [17-18]. Single phosphors directly yielding white emission are advantageous in comparison to a mixture of individual red, green, and blue phosphors as these are hampered by reabsorption of the blue light [17]. Keeping the above advantages in mind, and inspired by the possibility of fabricating the white light phosphor by single doping the host material with ions such as Tb^{3+} . The specific objectives are: Firstly, to synthesis ZnO by annealing $\text{Zn}(\text{OH})_2$ powders at 700 °C. Secondly, to synthesize and characterization of Tb^{3+} doped ZnO nanostructures, in order to study the effect of dopant (Tb^{3+}) on thermal analysis, structure, morphology and optical properties. The novelties of this work are: It was seen that the thermal stability was improved by annealing and doping (Tb-doping). It was also observed that the organic materials decreased with annealing and varying Tb molar concentrations. Lastly, morphology of un-doped ZnO consists of spherical nanoparticles, which changed in size and shape with an increase in the amount of Tb^{3+} dopant. When the Tb^{3+} ions were incorporated into ZnO, the spherical nanoparticles changed to mixed structures including the emergence of pyramids shape.

Experimental

Materials synthesis

All the chemicals used for the preparation of the nano-powders were of analytical grade. It includes zinc acetate ($\text{Zn}(\text{CH}_3\text{COO})_2 \cdot 2\text{H}_2\text{O}$), terbium nitrate ($\text{Tb}(\text{NO}_3)_3 \cdot 6\text{H}_2\text{O}$), thiourea ($(\text{NH}_2)_2\text{CS}$) (fuel) and ammonia (25% NH_3). All the precursors were dissolved in deionized water. During the preparation of the nano-powders, ammonia was used as a complexing agent. The schematic procedure for the preparation of the powder samples by the CBD is depicted in **Scheme 1**. The preparation of ZnO was carried out using

the following procedure: The ZnO nanoparticles were prepared by dissolving 0.46M of zinc acetate in 80 mL of deionized, thiourea of 0.18M in 80 mL of deionised water and lastly by dissolving 19.76 mL of ammonia in 80 mL of deionised water, respectively. The amount of solutions of zinc acetate, thiourea and ammonia was holding constant at ratio of 1:1:1 [4]. Then: 60 ml of the zinc acetate solutions were added in a beaker in the reaction bath. Followed by adding 60 ml of the thiourea solution in the same reaction bath and the mixture was stirred for a few seconds, lastly followed by adding 60 ml of an ammonia solution slowly into the mixture, while continues stirring for 2 minutes. The temperature of the bath was then allowed to increase up to 80 °C. After that the precipitates were formed and they were filtered immediately and washed with 60 ml of ethanol. The obtained particles were dried at ambient conditions (AC) for 3 days and. After dried they were annealed in air at 700 °C for 2 hours (h) using furnace. The powder samples were ready to be characterized using various characterization techniques. The synthesis of ZnO nanoparticles in the presence of the Tb^{3+} cations was performed similarly, but adding different molar concentrations of $\text{Tb}(\text{NO}_3)_3 \cdot 6\text{H}_2\text{O}$ to the $\text{Zn}(\text{CH}_3\text{COO})_2 \cdot 2\text{H}_2\text{O}$ precursor. The varied amount of $\text{Tb}(\text{NO}_3)_3 \cdot 6\text{H}_2\text{O}$ present in the precursor solution were: Tb mol%: 0.05, 0.09, 0.2, 0.4, 0.5, 0.6, 0.9, 1, 2, 3 and 4.



Scheme 1. Schematic illustration of the synthetic route of undoped and Tb-doped ZnO powders.

Characterization

Thermal analysis was carried out by thermogravimetric analyses (TGA) and differential thermogravimetric analyses (DTGA) were performed in a Perkin-Elmer TGA7 thermogravimetric analyzer. The samples were weighed masses of range 5–10 mg and were studied between 20 and 700 °C. The heating rate was 10 °C min^{-1} and the gas ($\text{N}_2 - 8\% \text{H}_2$) with a flow-rate of 120 $\text{cm}^3 \text{min}^{-1}$. The crystal structures of the samples were determined with a Bruker AXS Discover diffractometer with $\text{CuK}\alpha$ (1.5418 Å) radiation. The morphology of the prepared nanoparticles was determined with a scanning electron microscopy (SEM) using a Shimadzu model ZU SSX-550 Superscan coupled with an energy dispersive X-ray spectrometer

(EDS). The optical measurements were carried out in the 200 to 800 nm wavelength range using a Perkin Elmer UV/Vis Lambda 20 Spectrophotometer. Photoluminescence measurements were done on a Carry Eclipse Fluorescence Spectrophotometer system, equipped with a 150 W xenon lamp as the excitation source and SPEX 1870. All the samples used were in the powder form.

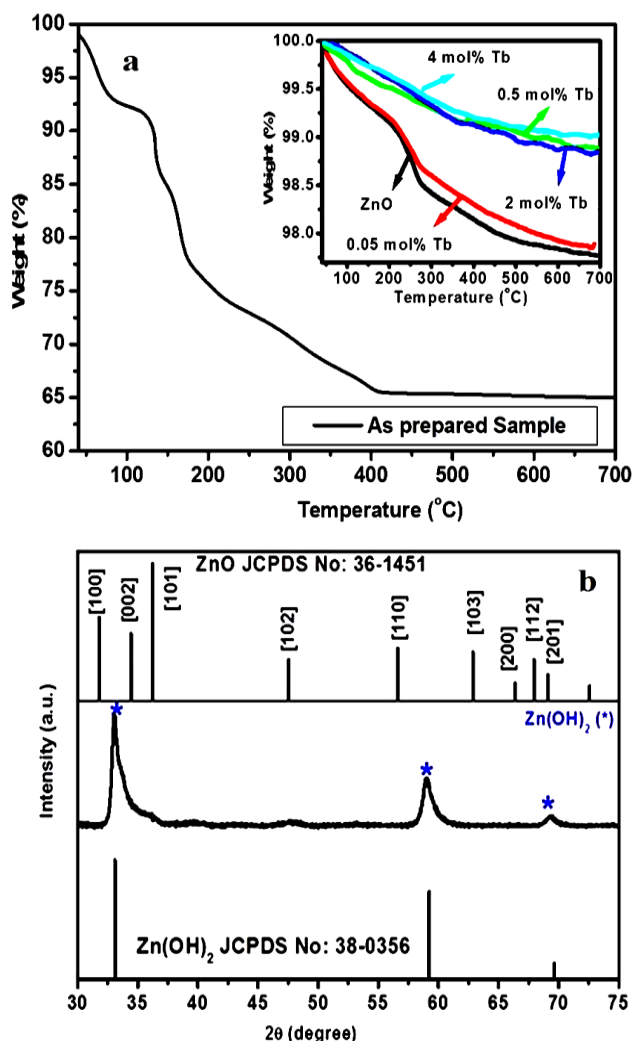


Fig. 1. (a) TGA measurements for as prepared, annealed and Tb-doped samples synthesized by CBD method. (b) X-ray powder diffraction patterns for Zn(OH)_2 nanoparticles synthesized for 2 min annealed at RT.

Results and discussion

The TGA of the as-prepared powders sample is shown in Fig. 1(a). The TGA traces of the as prepared shows an initial ~ 7 % weight loss from 40 – 92 °C, which may be attributed to the evaporation of ethanol and acetone. It is followed by gradual weight loss of 7.2 % from 92 - 145 °C, which corresponds to the physically absorbed water during the synthesis. The further 7.1% weight loss in the range 145 – 177 °C is assumed to be due to decomposition of unreacted zinc acetate. A gradual weight loss of ~ 12.1 % is observed in the range 177 - 400 °C and is assigned to dehydration of residual ammonia and nitrate ions, and in the range 400 - 700 °C there is 0.3 % weight loss which is due to the volatilization and combustible organic species present in the powders [19]. The slightly clear plateau is

observed in the temperature range 400 – 700 °C indicating that the ZnO powders starts to become thermally stable with just little weight loss. Hence the as-prepared ZnO powders were annealed at 700 °C for crystallization. Motloun *et al.* [20] indicated that the minimum annealing temperature to start forming metal oxide such as ZnO is 400 °C. Thus, the annealing temperature needs to be higher than 300 °C to remove all impurities and to improve the crystal structure of ZnO. The total weight loss for as prepared sample when heated from 40-700 °C was 34.1 wt %. The inset of Fig. 1 shows the TGA of un-doped and Tb-doped powders with different doping molar concentrations annealed at 700 °C for 2 h. Compared to as prepared sample, it can be seen that the thermal stability was improved by annealing and doping (Tb-doping). It was observed that the organic materials decreased with annealing and varying Tb molar concentrations. The overall weight loss for undoped powder sample annealed at 700 °C was 2.2 wt %. The weight loss for annealed Tb doped powder samples were 2.1, 1.1, 1.2 and 1 wt %, respectively. The yield is higher for the annealed Tb^{3+} -doped sample as compared to undoped ZnO sample. The observed high residual yield as molar concentration of Tb increases may be due to big molar mass of Tb nitrate compared to Zinc acetate.

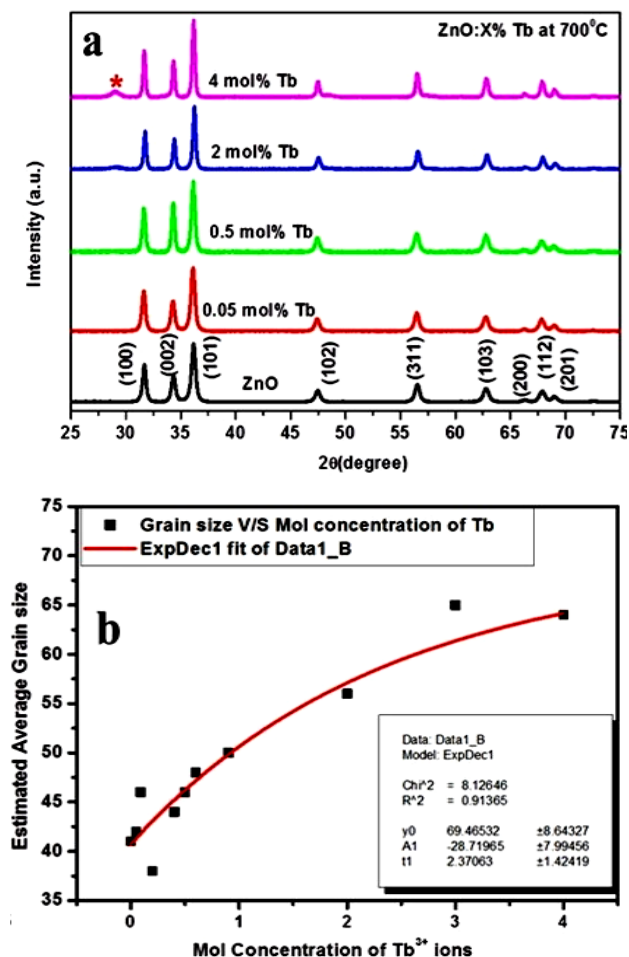


Fig. 2. (a) X-ray powder diffraction patterns for undoped and Tb-doped ZnO nanoparticles synthesized by CBD method and annealed at 700 °C. (b) The graph of average grain size versus the molar concentrations of Tb^{3+} ions for undoped and Tb-doped ZnO.

Crystal structures of the powders were characterized by XRD patterns. **Fig. 1(b)** shows the XRD pattern for as prepared sample dried at AC. A powder sample was just synthesized for 2 minutes and filtered immediately. We have seen that the final product is not ZnO but the zinc hydroxide ($\text{Zn}(\text{OH})_2$) as confirmed by standard JCPDS no: 38-0356. Thus the preparation process of undoped and Tb^{3+} -doped ZnO powders consists of three steps, *i.e.* chemical reaction, drying and annealing process. The Zn^{2+} ions first react with the OH^- originated from H_2O used as a solvent to form the precipitates at the bottom of a beaker, and then decompose into hexagonal wurtzite ZnO after further annealing at 700 °C. Annealing the as prepared sample at 700 °C, the $\text{Zn}(\text{OH})_2$ peaks disappeared at all as shown in **Fig. 2(a)**. The Figure shows the XRD patterns of undoped and Tb-doped ZnO samples annealed at 700 °C in air for 2 h. All the samples present sharp, narrow and well distinct peaks, which is an indication of crystalline nature. The main diffraction peaks are really indexed to wurtzite ZnO according to the JCPDS card no: 36-1451 with lattice parameters of $a = 0.3249$ nm and $c = 0.5206$ nm for both pure and Tb-doped ZnO samples. The estimated average lattice parameters are found to be $a = 0.3256$ nm and $c = 0.5215$. The estimated lattice parameters are slightly larger than those of bulk ZnO. All the peaks are used to estimate the lattice parameters. The increase of lattice parameters compared to bulk which are attributed to the inclusion of dopant ions into the Zn sites [4].

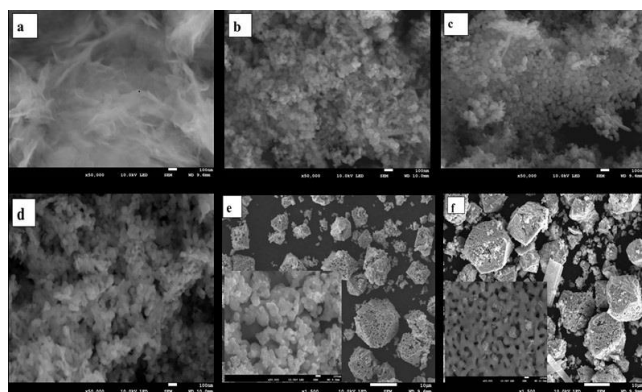


Fig. 3. SEM images of (a) $\text{Zn}(\text{OH})_2$, (b) ZnO annealed 700 °C, (c) ZnO:0.05 mol% Tb, (d) ZnO:0.5 mol% Tb, (e) ZnO:2 mol% Tb and (f) ZnO:4 mol% Tb.

No diffraction peaks from any other chemical species such as Tb nitrate are detectable when the doping molar concentration of Tb^{3+} ions is lower than 3 mol%. By carefully analysing the XRD patterns, we find that, when molar concentrations of Tb^{3+} ions are higher than 2 mol %, the peak at $2\theta = 29.1$ attributed to the terbium nitrate marked with asterisk (*) appears (confirmed with JCPDS card no: 80-1318), and the diffraction intensity of Tb nitrate increases with increasing Tb molar concentration. The average crystallite size of the undoped and Tb^{3+} -doped ZnO powders were estimated from the Full Width Half Maximum (FWHM) of the diffraction peaks using the Debye formula [21]. The major diffraction peaks for all the samples were chosen to estimate the average size of the nanocrystals by the least square method. The average

crystallite size of the as prepared samples was estimated to be 44 ± 2 nm. From **Fig. 2(b)**, it is clear that the estimated crystal size increases decay exponentially with an increase in molar concentration of Tb^{3+} ions [5]. The increase in the Tb^{3+} ions molar concentration at the ZnO matrix will increase the nucleation of the particles, which enhances the grain growth of Tb^{3+} -doped ZnO nanostructures.

Fig. 3(a-f) shows SEM micrographs of the powder samples. **Fig. 3(a)** shows the image of $\text{Zn}(\text{OH})_2$ powder dried at AC. Morphology of the sample consists of the flake-like. Annealing the $\text{Zn}(\text{OH})_2$ powder sample at 700 °C, shape changed to the spherical nanoparticle. It is clear that the morphology is agglomerated and uniform in size. With the incorporation of Tb^{3+} ions into annealed ZnO, the nanoparticles increase in size slightly and clustered more as seen from **Fig. 3(c-d)**. In **Fig. 3(e)** for ZnO doped with 2 mol % Tb^{3+} , it is clear that the nanoparticles changed to the pyramids shape. When the Tb^{3+} ions molar concentration was increased further to 4 mol %, those pyramids increased in size slightly and there was some mixture of block-like shape. Those pyramids are not uniform in size and are not clustered. Zooming on one of the pyramid it is clear that they are build-up of spherical nanoparticles which are distributed uniformly and clustered as shown as an inset in **Fig. 3(e-f)**. The size of the pyramids structure from the ZnO doped with 4 mol% Tb^{3+} ions were large, in the order of about 10 μm . Energy-dispersive x-ray spectroscopy (EDX) of the powder samples suggests the existence of Zn, Tb, O and C (which is not shown here). From the spectra it was observed that the Tb^{3+} ions became visible for the higher molar concentration of dopant. No Tb^{3+} was measured for the lower (< 1 mol% Tb^{3+}) concentration of Tb doped.

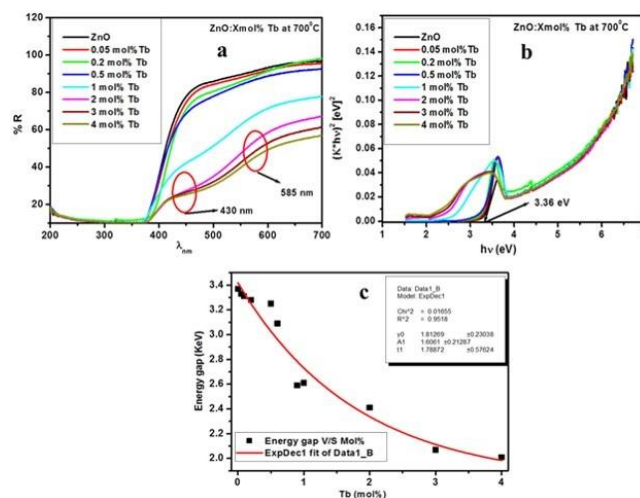


Fig. 4. (a) The reflectance spectra, (b) Plot to determine the band gap energy of the undoped and Tb^{3+} -doped ZnO nanoparticles and (c) Dependence of the band gap energies of the ZnO on the amount of Tb^{3+} ion dopants.

The UV-visible absorption spectra of the as prepared samples are illustrated in **Fig. 4(a)**. The Tb-doping has no significant effect on reflectance of ZnO in the visible region but drastically improves the absorption in the UV-region. It is clear that the position of the absorption edge shifts to higher wavelength with an increase of the doping

concentration of Tb^{3+} . It was observed that at lower molar concentrations of Tb^{3+} the absorption edges are homogeneous. Increasing the Tb molar concentration further the absorption edges are not homogeneous. At higher molar concentration of Tb there were two absorption bands at around 430 and 585 nm. The two absorption bands may be due to non-uniform morphology at higher molar concentration of Tb^{3+} as observed from SEM analysis.

The energy band gap of these materials was estimated using the Kubelka-Munk function as shown in Fig. 4(b) [22]. The band gap energy for undoped ZnO nanoparticles was estimated to be 3.36 ± 0.09 eV which is in the same order than bulk ZnO [1]. From Fig. 4(c), it is clear that the estimated band gap energies decay with an increase in the amount of Tb molar concentrations. The shift of absorption edges to higher wavelengths and the decrease in the band gap energy with an increase in Tb molar concentrations may be due to the estimated crystallite sizes that are increasing with an in the amount of dopant as confirmed by XRD and SEM analysis [23]. Lastly, might be due to the presence of defect states and disorder due to the Tb^{3+} ions doping [4].

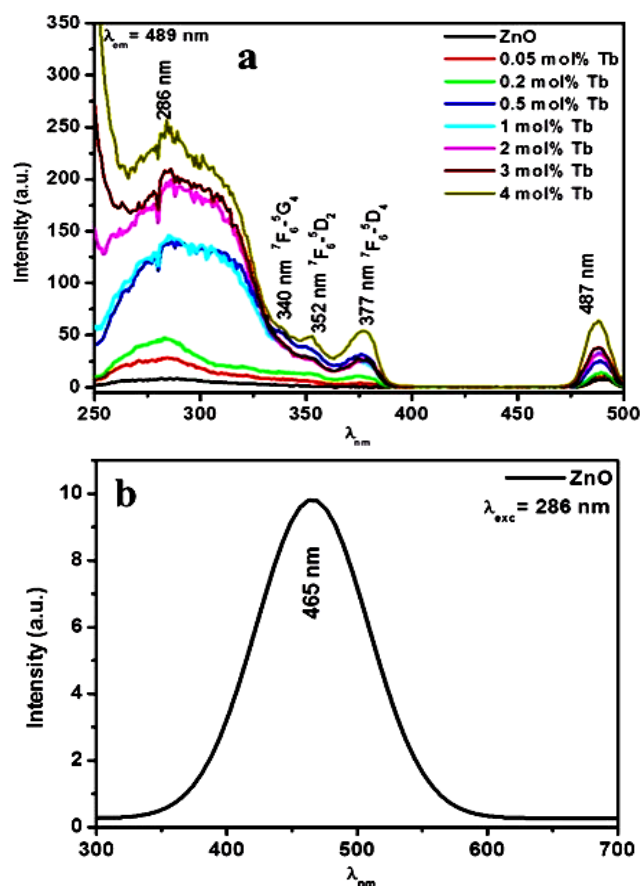


Fig. 5. (a) Excitations spectra for undoped and Tb-doped ZnO nanoparticles at different molar concentrations of Tb^{3+} ions with emission wavelength of 489 nm using Xenon lamp, and (b) Photoluminescence spectra for undoped ZnO nanoparticles showing the emission within the UV-visible range when excited at 286 nm using a Xenon lamp.

The photoluminescence (PL) measurement of the ZnO nanoparticles was carried out at room temperature using a Xenon lamp. Fig. 5(a) depicts the room temperature excitation spectrum of the undoped and Tb-doped ZnO

nanoparticles. The undoped ZnO structures display broad bands in the UV region with peaks at around 286 nm [24-25]. By increasing the molar concentration of Tb^{3+} ions, the three peaks start to emerge at around 340, 352 and 377 nm which correspond to the electronic transition of Tb^{3+} ions from the ground state 7F_6 to excited states 5G_4 , 5D_2 and 5D_4 , respectively [26]. The peaks intensities increase with an increase in the molar concentration of Tb^{3+} ions. The excitation signals from these states indicate that there is an emitting state within the bandgap. The PL emission spectrum of undoped ZnO nanoplates is shown in Fig. 5(b). The undoped ZnO nanoplate exhibits a broad band in the region between 350 and 700 nm with one prominent maximum at 465 nm.

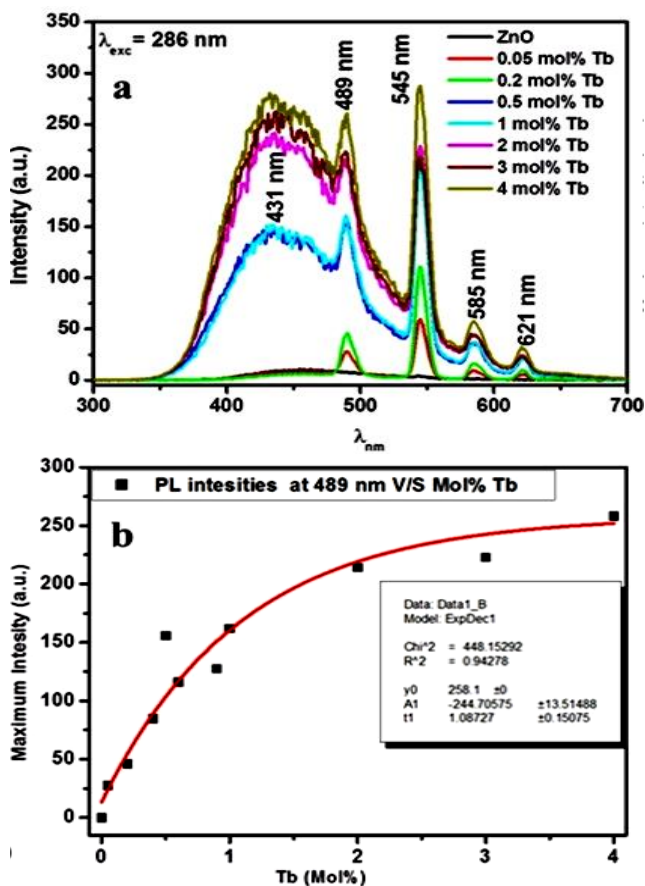


Fig. 6. (a) Photoluminescence spectra for undoped and Tb-doped ZnO nanoparticles showing all the emissions within the UV-visible range when excited at 286 nm using a Xenon lamp and (b) Dependence of emission intensity of the ZnO-Tb nanoparticles on the concentration of Tb at emission wavelength of 489 nm.

The broad emission has been assigned to the excitons on the surface of ZnO nanoparticles [27]. The PL emission spectra of ZnO nanoparticles in the presence of different molar concentration of Tb^{3+} at ambient temperature are shown in Fig. 6(a). It was observed that the presence of Tb^{3+} ions affect the luminescence wavelength and intensity. Firstly, the luminescence band of undoped ZnO at around 465 nm diminished with an increase in the amount of Tb content and the luminescence band due to Tb^{3+} emerges with an increase in the molar concentration of Tb^{3+} ions. This behavior may be due to a well-known energy transfer

from host (ZnO) to Tb^{3+} ions [6]. The doped samples showed emission peaks centred at 431, 489, 545, 585 and 621 nm for all Tb molar concentrations. These blue and green emission peaks can be associated with the intra-4f transitions of Tb^{3+} in particular, $^5D_3 \rightarrow ^7F_4$, $^5D_4 \rightarrow ^7F_6$, $^5D_4 \rightarrow ^7F_5$, $^5D_4 \rightarrow ^7F_4$ and $^5D_4 \rightarrow ^7F_3$ transitions, respectively [28]. Secondly, it was observed that the luminescence intensity increases with an increased in molar concentration of Tb^{3+} ions. The dependence of the luminescence intensity (489 nm) of the nanostructures on the concentration of Tb is illustrated in Fig. 6(b). It can be seen clearly that the luminescence intensity of the nanoparticles in the visible region growth nearly exponential with Tb content. The group of Lang *et al.* [29] observed that the luminescence band of green emission of ZnO increases in luminous intensity with an increase in the mol % of Ce^{3+} ions. The improved intensity of the green emission was attributed to increases in the density of defects, which could be due to the oxygen vacancy introduced by the existence of Ce impurities in ZnO nanorods [29]. In our study, similarly behavior was observed were the luminescence intensity of Tb-doped ZnO increased with an increase in Tb^{3+} molar concentrations. The improved Tb^{3+} emission intensity may be attributed to the increase in the activator (Tb^{3+}) ions. More interestingly, when the amount of Tb^{3+} molar concentration is increased, the emission color is tuned from bluish to greenish. Generally, the emission color of the single doped phosphor can be tuned by changing the Tb^{3+} mol%, which suggests that this kind of novel phosphor can meet the wide range of application requirements such in blue to green LEDs.

Conclusion

Tb^{3+} -doped ZnO nanopowders were successfully synthesized by the chemical bath process and post-annealed at 700 °C for 2 h. TGA showed the best annealing temperature for ZnO is 700 °C. The morphology, the crystalline quality and the optical properties of the Tb^{3+} -doped ZnO nanoparticle can be changed by increasing the Tb^{3+} doping level. The XRD patterns indicated that a high crystallinity in the hexagonal lattice of the undoped and Tb^{3+} -doped ZnO nanoparticles was obtained. SEM images depict homogenous spherical nanoparticles for undoped ZnO. After doping the spherical nanoparticles became clustered and changed in shape, especially for Tb concentration higher than 2 mol %. EDS confirmed all the expected elements. UV spectroscopy showed that the band gap energy of the doped ZnO nanoparticles decreased with an increase in the molar concentration of Tb. The PL spectra showed that the emission intensity of the Tb^{3+} -doped ZnO samples increased with the increase of the Tb^{3+} content compared to the undoped ZnO. These results revealed that the ZnO particles changed from spherical to pyramids shape by varying the amount of Tb^{3+} molar concentrations. Future work will focus on the synthesis of the Tb^{3+} doped ZnO nanostructures by varying the solvents. The effect of solvents on the structure, morphological and optical properties of Tb^{3+} doped ZnO nanocrystals will be studied.

Acknowledgements

The author would like to acknowledge the National Research Foundation (NRF), Knowledge Interchange and Collaboration (KIC), the University of the Free State, Prof Birhanu F. Dejene, Dr Setumo V. Motloung for financial support. Also thankful to Prof. Tshwafo E. Motaung and Dr. Shanganyane Hlangothi for doing TGA and DTGA. Prof Hendrik C. Swart for XRD and SEM.


Author's contributions

I (Lehlohonolo F. Koao, I'm the one who have written the manuscript and did data analysis for the whole manuscript. I have Performed the experiments for SEM; EDS; PL; UV and XRD. TGA and DTGA data was collected by Prof. Tshwafo E. Motaung and Dr. Shanganyane Hlangothi. Prof Birhanu F. Dejene, Dr Setumo V. Motloung and Prof Hendrik C. Swart have modified the paper.

Reference

- Yang L.; Tang Y.; Hu A.; Chen X.; Liang K.; Zhang L. *Physica B*. **2010**, 403, 2234.
DOI: [10.1016/j.physb.2007.12.013](https://doi.org/10.1016/j.physb.2007.12.013)
- Dejene F. B.; Ali A. G.; Swart H. C.; Botha J. R.; Roro K.; Coetsee E.; Biggs M. M. *Cent. Eur. J. Phys.* **2011**, 9(5), 1321.
DOI: [10.2478/s11534-011-0050-3](https://doi.org/10.2478/s11534-011-0050-3)
- Dijken A.V.; Mulenkamp E. A.; Vanmaekelbergh D.; Meijerink A. *J. Lumin.* **2000**, 90, 123.
DOI: [10.1016/S0022-2313\(99\)00599-2](https://doi.org/10.1016/S0022-2313(99)00599-2)
- Koao L. F.; Dejene F. B.; Kroon R. E.; Swart H. C. *J. Lumin.* **2014**, 147, 89.
DOI: [10.1016/j.jlumin.2013.10.045](https://doi.org/10.1016/j.jlumin.2013.10.045)
- Kumar V.; Som S.; Kumar V.; Kumar V.; Ntwaeaborwa O. M.; Coetsee E.; Swart H. C. *Chem. Eng. J.* **2014**, 255, 552.
DOI: [10.1016/j.cej.2014.06.027](https://doi.org/10.1016/j.cej.2014.06.027)
- Bayan S.; Das U.; Mohanta D. *Phys. Status. Solidi A.*, **2010**, 207 (8): 1863.
DOI: [10.1002/pssa.200925525](https://doi.org/10.1002/pssa.200925525)
- Anh T. K.; Loc D. X.; Tu N.; Huy P.T.; Tu L. M. A.; Minh L. Q. *J. Photonics*. **2014**, 2014, 5.
DOI: [10.1155/2014/684601](https://doi.org/10.1155/2014/684601)
- Rajeswari Y. N.; Chandra B. A. *Prog. Nanotechnol. Nanomatt.* **2013**, 2, 20.
- Karunakaran C.; Gomathisankar P.; Manikandan G. *Mater. Chem. Phys.* **2010**, 123, 594.
DOI: [10.1016/j.matchemphys.2010.05.019](https://doi.org/10.1016/j.matchemphys.2010.05.019)
- Khataee A.; Soltani R. D. C.; Karimi A.; Joo S. W. *Ultrason. Sonochem.* **2015**, 23, 230.
DOI: [10.1016/j.ultsonch.2014.08.023](https://doi.org/10.1016/j.ultsonch.2014.08.023)
- Geng J.; Song G. H.; Zhu J. J. *J. Nanomater.* **2012**, 2012, 5.
DOI: [10.1155/2012/317857](https://doi.org/10.1155/2012/317857)
- Zong Y.; Li Z.; Wang X.; Ma J.; Yi Menn. *Ceram. Int.* **2014**, 40, 10382.
DOI: [10.1016/j.ceramint.2014.02.123](https://doi.org/10.1016/j.ceramint.2014.02.123)
- Roy B.; Chakrabarty S.; Mondal O.; Pal M.; Dutta A. *Mater. Charact.* **2012**, 70, 7.
DOI: [10.1016/j.matchar.2012.04.015](https://doi.org/10.1016/j.matchar.2012.04.015)
- Khataee A.; Karimi A.; Oskoui S. A.; Soltani R. D. C.; Hanifehpour Y.; Soltani B.; Sang Woo Joo S. W. *Ultrason. Sonochem.* **2015**, 22, 381.
DOI: [10.1016/j.ultsonch.2014.05.023](https://doi.org/10.1016/j.ultsonch.2014.05.023)
- Reisfeld R.; Gaft M.; Saraidarov T.; Panczer G.; Zelner M. *Mater. Lett.* **2000**, 45, 156.
DOI: [10.1016/S0167-577X\(00\)00096-3](https://doi.org/10.1016/S0167-577X(00)00096-3)
- Zhao S.; Wang L.; Yang L.; Wang Z. *Physica B*. **2010**, 405, 3204.
DOI: [10.1016/j.physb.2010.04.049](https://doi.org/10.1016/j.physb.2010.04.049)
- Lorbeer, C.; Mudring, A.-V. *J. Phys. Chem. C*. **2013**, 117, 12238.
DOI: [10.1021/jp312411f](https://doi.org/10.1021/jp312411f)
- Zhang, Y.; Zhu, Z.; Qiao, Y. *Mat. Lett.* **2013**, 93, 11.
DOI: [10.1016/j.matlet.2012.11.068](https://doi.org/10.1016/j.matlet.2012.11.068)
- Bagheri S.; Chandrappa K. G.; Hamid S. B. A. *Der. Pharma. Chemica*. **2013**, 5, 270.
DOI: [10.1155/2011/853832](https://doi.org/10.1155/2011/853832)
- Motloung S. V.; Dejene B. F.; Swart H. C.; Ntwaeaborwa O. M. *J. Sol-Gel Sci. Technol.* **2014**, 70, 427.
DOI: [10.1007/s10971-014-3302-z](https://doi.org/10.1007/s10971-014-3302-z)
- Lavand A. B.; Malghe Y. S. *Adv. Mater. Lett.* **2015**, 6(8), 700.
DOI: [10.5185/amlett.2015.5800](https://doi.org/10.5185/amlett.2015.5800)

22. Koao L. F.; Dejene F. B.; Swart H. C. *Mater. Sci. Semicond. Process.* **2014**, 27, 40.
DOI: [10.1016/j.mssp.2014.06.009](https://doi.org/10.1016/j.mssp.2014.06.009)
23. Vidhya Raj D. J.; Justin Raj. C.; Jerome Das. S. *Superlattices Microstruct.* **2015**, 85, 281.
DOI: [10.1016/j.spmi.2015.04.029](https://doi.org/10.1016/j.spmi.2015.04.029)
24. Taunk P. B.; Das R.; Bisen D.P.; Tamrakar R. K. *J. Radiat. Res. Appl. Sci.* **2015**, 8, 438.
DOI: [10.1016/j.jrras.2015.03.006](https://doi.org/10.1016/j.jrras.2015.03.006)
25. Thankappan A.; Hari M.; Mathew S.; Joseph S. A.; Rolf E.; Bora D.; Braun A.; Nampoore V. P. N. *Physica E.* **2012**, 44, 2123.
DOI: [10.1016/j.physe.2012.06.026](https://doi.org/10.1016/j.physe.2012.06.026)
26. Sontakke. A.D.; Biswas. K.; Annapurna. K. *J. Lumin.* **2009**, 129, 1355.
DOI: [10.1016/j.jlumin.2009.06.027](https://doi.org/10.1016/j.jlumin.2009.06.027)
27. Singh L. R. *Mater. Sci. Applicat.* **2015**, 6, 278.
DOI: [10.4236/msa.2015.64032](https://doi.org/10.4236/msa.2015.64032)
28. Bajaj N. S.; Omanwar S. K. *J. Lumin.* **2014**, 153, 290.
DOI: [10.1016/j.jlumin.2014.03.053](https://doi.org/10.1016/j.jlumin.2014.03.053)
29. Lang J.; Han Q.; Yang J.; Li C.; Li X.; Yang L.; Zhang Y.; Gao M.; Wang D.; Cao J. *J. Appl. Phys.* **2010**, 107, 4.
DOI: [10.1063/1.3318613](https://doi.org/10.1063/1.3318613)



A Monthly Journal

Publish your article in this journal

Advanced Materials Letters is an official international journal of International Association of Advanced Materials (IAAM, www.iaamonline.org) published monthly by VBRI Press AB from Sweden. The journal is intended to provide high-quality peer-review articles in the fascinating field of materials science and technology particularly in the area of structure, synthesis and processing, characterisation, advanced-state properties and applications of materials. All published articles are indexed in various databases and are available download for free. The manuscript management system is completely electronic and has fast and fair peer-review process. The journal includes review article, research article, notes, letter to editor and short communications.

Copyright © 2016 VBRI Press AB, Sweden

www.vbripress.com/aml